Effect of Boundary Streamline Deflection Angle on Detonation Propagation

Carlos Chiquete, Mark Short, Chad D. Meyer and James J. Quirk
Los Alamos National Laboratory
Los Alamos, New Mexico, USA

1 Introduction

We are concerned with condensed-phase high explosive (HE) detonation performance, particularly in engineering applications where the HE is surrounded by a range of materials including metals and plastics. A key feature of detonations is that the high post-shock pressures cause the yielding of any confining material. A lateral flow component then develops within the reaction zone. This results in a curved detonation front which tends to slow the propagation of the wave because the sonic locus moves toward the front, relative to the fully confined detonation wave, cutting off some of the energy release from supporting the front propagation. In the steady propagation context represented in Fig. 1a, the region between the front and the steady state sonic locus, which supports the wave propagation, is known as the detonation driving zone (DDZ).

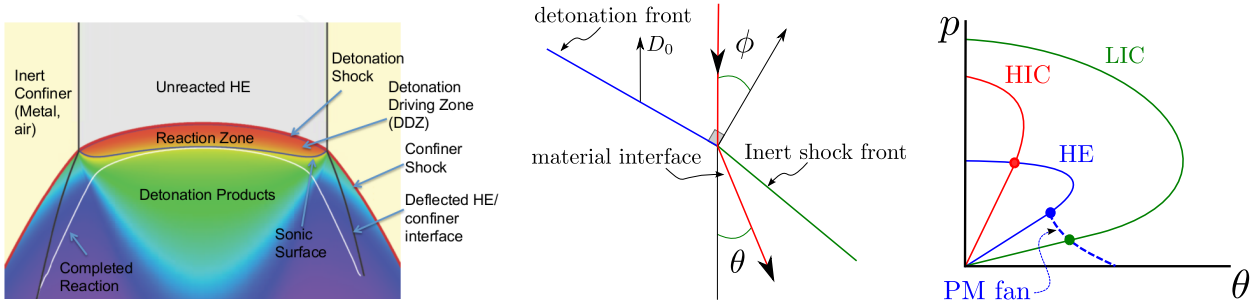

(a) (b) (c)

Figure 1: (a) Schematic of two-dimensional detonation wave propagation in a weak confinement configuration [1]. (b) Shock polar analysis geometry. (c) Representation of shock polars for HE and both HICs and LICs (in $p - \theta$ plane).

The extent of the slowing effect depends on the density and impedance of the confining inert material. High impedance confiners (HIC) (e.g. metals) lessen this effect relative to low impendance confiners (LIC) (e.g. plastics). In particular, for weak enough confiners, the flow near the edge of the explosive becomes sonic,

Correspondence to: chiquete@lanl.gov

isolating the DDZ from the inert material and setting a minimum steady phase speed. This steady-state wave propagation configuration is referred to as "unconfined" (cf. Fig 1a).

A shock polar analysis (SPA) can help distinguish the various gasdynamic reflection patterns that result from the shock intersecting the HE-confiner material boundary [2]. Figure 1b shows the configuration of the shock front in both inert and HE and the deflected material interface (note that all are assumed to be straight in the SPA). Using the oblique shock relations and equation-of-state (EOS) definitions specific to the HE and inert confiner, "shock polar" diagrams can be drawn in the pressure (p) and streamline turning angle (θ) plane as in Fig. 1c. A point match can be sought in these two quantities for the pair of materials to produce a predicted interface deflection and matching pressure across the material interface along with shock normal angles (ϕ) for both inert and HE.

Two main types of interaction are highlighted here. For a HIC, the shock polar tends to lie above the HE counterpart, leading to a "strong" match as shown in Fig. 1c in the intersection of the red and blue lines. The result is a subsonic intersection point and flow in the HE, meaning the post-shock flow is influenced by the specific HIC. For a LIC, no direct match in the $p - \theta$ plane is possible as shown by the green and blue curves in Fig. 1c (LIC polar lies below the HE counterpart). In this case, the "weak" point-match solution requires a Prandtl-Meyer (PM) expansion fan connecting the HE pressure down to the lower LIC level. This amounts to a sonic flow (in the traveling frame) at the intersection point of the detonation shock and material interface, isolating the flow in the DDZ to the specific flow conditions in the LIC.

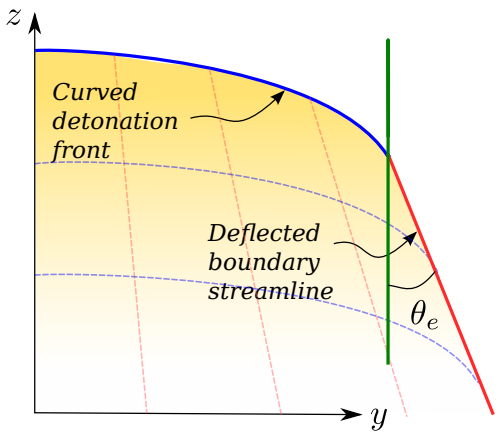

Figure 2: Detonation propagation geometry with linear side boundary streamline deflection.

The focus of our work here is to systematically investigate the effect of boundary streamline deflection on detonation propagation. To this end, we perform reactive flow simulations using a simple HE model and simplified computational geometries where we enforce a straight boundary streamline in the flow at a prescribed deflection angle (cf. Fig. 2). The steady-state phase velocity and DDZ bounds are extracted from the calculations as a function of the imposed deflection angle. Finally, we compare the unconfined steady-state phase velocity variation with sonic shock-normal angle from these simulations to the corresponding SPA predictions.

2 Model and numerical method

We used a simple HE model (Tait stiffened gas EOS, and one-step pressure-sensitive reaction rate),

$$e_{int} = (p + a)/\rho\Gamma - \lambda q, \Lambda = kp(1 - \lambda)^{1/2}, \tag{1}$$

where e_{int} is the specific internal energy, p is pressure, ρ is the density, λ is the single reaction progress variable and $\Gamma = 2.0$ and $q = 0.0324$ cm$^2/\mu$s^2. Note that the EOS parameter a was varied between $a = 0.0$ and $a = 0.128$ Mbar in the computations and $a = 0.0$ Mbar represents the ideal-gas case. For the reaction rate, we varied k with a, i.e. $k = 5.707$ and $k = 5.136$ μs^{-1} Mbar^{-1} for $a = 0.0$ and $a = 0.128$ Mbar, respectively.

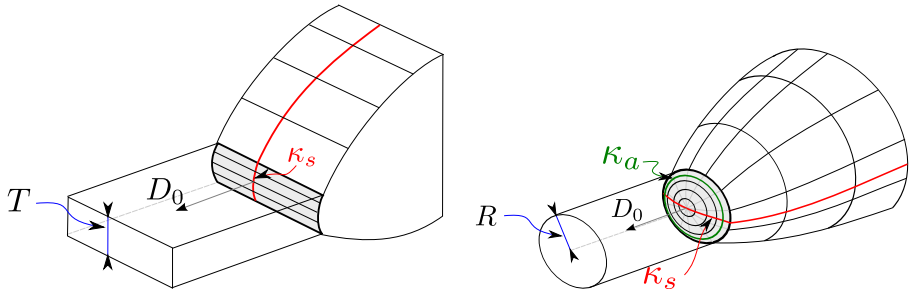

Figure 3: Schematic of computation geometries (based on Higgins [5]). The front slab curvature component κ_s appears in red and the axisymmetric contribution to the total curvature κ_a appears in green (only in the ratestick geometry).

The Reactive-Euler equations were solved using a shock-attached approach developed by [3] and using the side boundary streamline deflection approach originated in Romick and Aslam [4]. The simulations utilized either a slab (2D planar) or ratestick (axisymmetric cylindrical) geometry (cf. Fig. 3). The present work used a finite-volume, second-order in time and space scheme to solve the transformed set of conservation equations. The implementation of this methodology is detailed in Chiquete *et al* [6]. Each computation was initiated with zero deflection and gradually ramped up to the chosen value of θ_e. The initial solution field was the Zel'dovich-von Neumann-Döring (ZND) profile, i.e. the 1D steady-state, and each computation was integrated to steady state.

3 Results

The deflection angle of the imposed streamline (see Fig 2a), θ_e, was varied over a range of values for different a and lateral domain lengths or "charge-sizes". Figure 4 illustrates the effect of increasing the streamline deflection angle on the steady-state DDZ bounds (i.e. the region bounded by the shock front and sonic locus) specifically for a slab simulation and $a = 0.0$ Mbar and $T = 3.16$ cm. The DDZ and the phase velocity (noted in each legend entry) eventually begin to converge given a large enough deflection.

The shock-attached DDZ results were compared to an adaptive mesh refinement (AMR) simulation, employing shock-capturing, that modeled a slab of HE surrounded by low impedance plastic [6–8]. Figure 4 shows a reasonable comparison between the two very different methodologies. In particular, the phase speed for the AMR simulation was 0.6313 cm/μs while the shock attached simulations approach a value

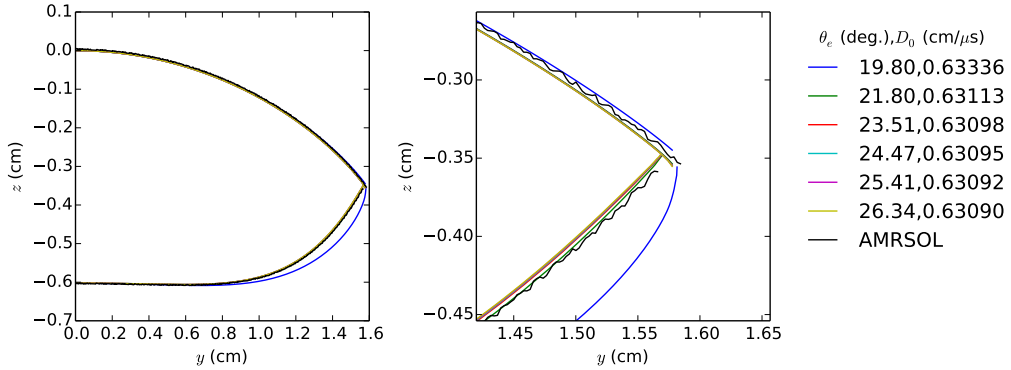

Figure 4: The DDZ structure as function of θ_e in the shock-attached simulations ($a = 0.0$ for 32 per ZND half-reaction zone (HRL)) and a comparison to an AMR multi-material simulation [7, 8] (denoted here as AMR_SOL) which used a maximum of 40 points per ZND HRL.

of 0.6309 cm/μs, a difference of just 4 m/s. This agreement in phase velocity, front and sonic locus location implies that given a large enough deflection angle, the shock-attached methodology approximates the weakly confined HE reaction zone dynamics described in section 1.

The limiting behavior of the phase velocity as function of θ_e is shown in Fig. 5 for slab simulations spanning two different HE domain sizes and two values of a. The sensitivity of D_0 to θ_e for smaller deflection (when the flow is subsonic near the boundary) was much higher than at large deflections. As suggested by the SPA analysis, the reaction zone dynamics eventually become "unconfined" in the sense that past a certain level of streamline divergence, the steady state propagation dynamics are no longer influenced by further increasing θ_e. Comparing the smaller T case on the left to the larger case on the right for each a value, the smaller charge shows a greater range in phase velocity for the same range of θ_e. Note that when deflection angles were increased beyond the plotted range in Fig. 5, additional sharply-varying flow structures appear that are required to turn the flow to the imposed boundary streamline angle.

The phase velocity variation with θ_e shown in Fig. 5 suggests there is a limiting behavior where the phase velocity eventually becomes independent of θ_e. We extracted this limit by approximating the derivative of D_0 with θ_e and looking for the value of θ_e (and corresponding D_0) which met our chosen limit threshold (i.e. $dD_0/d\theta_e \leq 10^{-5}$ cm/μs/deg.). Figure 5 shows the generated limit value of D_0 for each case with dashed horizontal lines. Given these limiting or "unconfined" detonation phase velocities and picking out the sonic-shock normal angle (ϕ_s) from each front calculation, Fig. 6 plots these two quantities for both HE geometries and two values of a. Additionally, the corresponding SPA trend is plotted in the solid line. Firstly for the $a = 0.0$ or ideal-gas case, the computations show some sensitivity of the shock-normal angle to the phase speed. In contrast, the SPA predicts a constant ϕ_s independent of D_0. Note that this this is a consequence of the applied strong shock limit in the SPA for condensed-phase HEs. However, the difference in ϕ_s for different values of D_0 betweeen the SPA and the computation only amounts to fractions of a degree. For the non-ideal EOS case, $a = 0.128$ Mbar, the computations and theoretical analysis show a similar level of variation of ϕ_s with D_0. However, the differences between theory and computations now grow to a few degrees. Note that the SPA crucially assumes no curvature in the detonation front at the charge-edge but Fig. 7 shows that curvature is sharply maximized precisely in this region. Finally, Fig. 6 shows that the calculated ϕ_s are close for both simulated HE geometries.

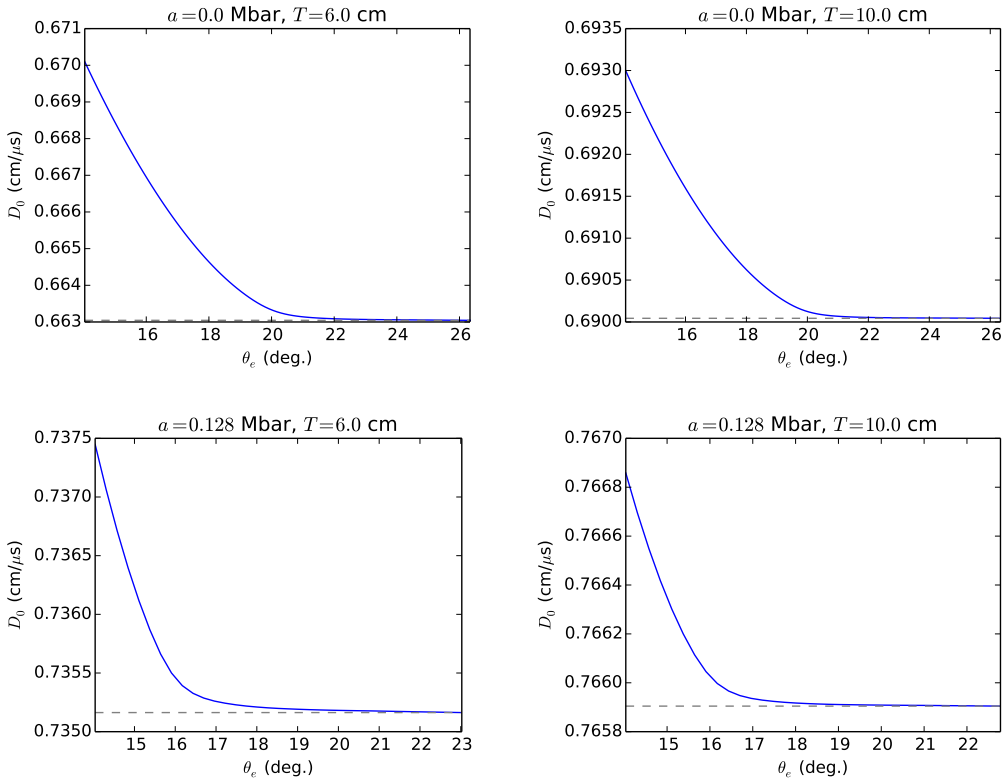

Figure 5: Limiting behavior of phase velocity as function of θ_e for $a = 0.0$ and $a = 0.128$ Mbar and two different simulation slab sizes.

4 Summary and future work

We investigated the effect of boundary streamline deflection on the reaction zone structure in simplified reactive flow simulations of detonation propagation. We found that the detonation propagation is especially sensitive to the lower range of simulated streamline deflection angle where the detonation is confined. We then compared the predictions of the SPA to the calculations, finding a significant difference for the non-ideal EOS HE model.

In future work, more realistic HE EOS models like Davis Reactants and Products will be analyzed using parameter sets representing real explosives. Also, reaction rates representing ideal, insensitive and non-ideal explosives should be explored in this context. The effect of more complicated boundary streamline shapes will be explored as well.

References

[1] Bdzil JB, Aslam TD, Henninger R, Quirk JJ. (2003) High-explosives performance: understanding the effects of a finite-length reaction zone. Los Alamos Science 28, 96-110.

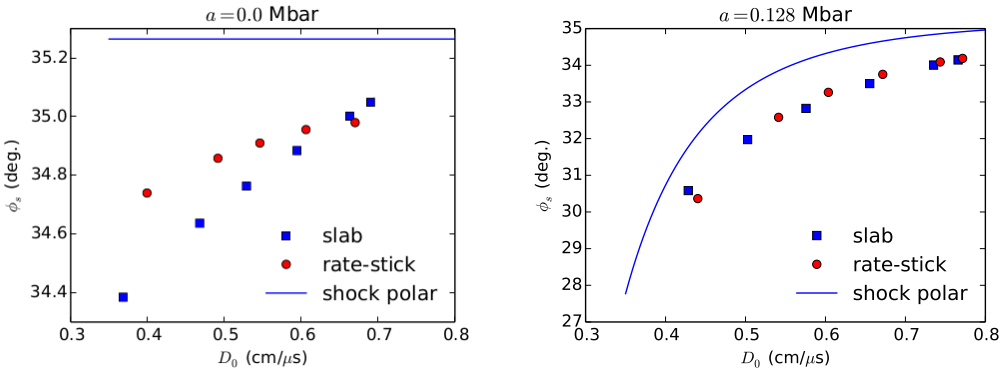

Figure 6: The dependence of the sonic shock normal angle on the unconfined D_0 for computations in both simulation geometries and the shock polar analysis analogue. The difference in the computed shock normal angles between the two simulation geometries increases for the lower range in phase velocity.

[2] Bdzil JB, Stewart DS. (2011). Theory of detonation shock dynamics. Detonation Dynamics: Shock Waves Science and Technology Library 6, 373-453.

[3] Henrick AK. (2008). Shock-fitted numerical solutions of one-and two-dimensional detonation. PhD thesis, University of Notre Dame.

[4] Romick CM, Aslam TD. (2014). Two-dimensional detonation propagation using shock fitting. In Proc. 15th Intl. Symp. on Detonation, pages 380–389. Office of Naval Research.

[5] Higgins AJ. (2014). Discrete effects in energetic materials. J. Phys.: Conf. Series, 500(5):052016.

[6] Chiquete C, Meyer CD, Short M & Quirk JJ. (2017). Calibration methodology for synchronized programmed burn detonation wave propagation. Combust. Flame. p. submitted.

[7] Quirk JJ. (1996). A parallel adaptive grid algorithm for computational shock hydrodynamics. Appl. Num. Math. 20 (4), 427453.

[8] Quirk JJ. (2007). amr sol:multimat. Tech. Rep. LA-UR-07-0539. Los Alamos National Laboratory.

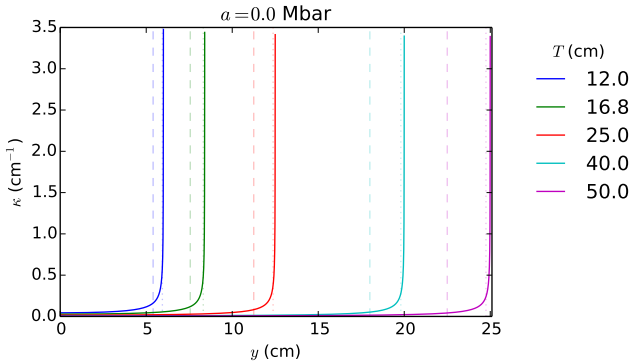

Figure 7: Calculated curvature across slab front for $a = 0.0$ Mbar, for a series of domain sizes.